Earth Syst. Sci. Data Discuss., doi:10.5194/essd-2016-14, 2016
Manuscript under review for journal Earth Syst. Sci. Data
Published: 6 June 2016

Open Access Earth System Science Data Discussions

The integrated water balance and soil data set of the Rollesbroich hydrological observatory

Wei Qu[1], Heye R. Bogena[2,*], Johan A. Huisman[2], Marius Schmidt[2], Ralf Kunkel[2], Ansgar Weuthen[2], Bernd Schilling[2], Jürgen Sorg[2] and Harry Vereecken[2]

[1] Institute for Applied Geophysics and Geothermal Energy (E.ON Energy Research Center), Mathieustraße 10, 52074 Aachen, Germany

[2] Institute of Bio- and Geosciences: Agrosphere (IBG-3), Jülich Research Centre, 52425 Jülich, Germany.

* Corresponding author (h.bogena@fz-juelich.de)

Earth Syst. Sci. Data Discuss., doi:10.5194/essd-2016-14, 2016
Manuscript under review for journal Earth Syst. Sci. Data
Published: 6 June 2016

Abstract

The Rollesbroich headwater catchment located in Western Germany is a densely instrumented hydrological observatory and part of the TERENO (Terrestrial Environmental Observatories) initiative. The measurements acquired in this observatory present a comprehensive dataset that contains key hydrological fluxes in addition to important hydrological states and properties. Meteorological data (i.e. precipitation, air temperature, air humidity, radiation components, and wind speed) are continuously recorded and actual evapotranspiration is measured using the eddy covariance technique. Runoff is measured at the catchment outlet with a gauging station. In addition, spatio-temporal variations in soil water content and temperature are measured at high resolution with a wireless sensor network (SoilNet). Soil physical properties were determined using standard laboratory procedures from samples taken at a large number of locations in the catchment. This comprehensive data set can be used to validate remote sensing retrievals and hydrological models; to improve the understanding of spatial temporal dynamics of soil water content; to optimize data assimilation and inverse techniques for hydrological models; and to develop upscaling and downscaling procedures of soil water content information. The complete data set is freely available online (http://www.tereno.net).

Earth Syst. Sci. Data Discuss., doi:10.5194/essd-2016-14, 2016
Manuscript under review for journal Earth Syst. Sci. Data
Published: 6 June 2016

Open Access Earth System Science Data Discussions

1. Introduction

Climate and land use changes are taking place on different spatial and temporal scales affecting all environmental compartments. Soil water content is known to be a major control for evapotranspiration, precipitation-runoff response, and heat transfer between soil and atmosphere, and it plays an essential role for climate projections, weather and flood forecasting, water and soil resources management, agriculture, and water quality control (Albertson and Kiely, 2001; Betts et al., 1996; Crow et al., 2005; Robinson et al., 2008; Vereecken et al., 2008; Western et al., 2002). However, the highly heterogeneous pattern of soil water content leading to complex and scale-dependent patterns of water, energy, and matter fluxes makes it challenging to predict terrestrial system responses for both scientists and policymakers (Jaeger and Seneviratne, 2011; Seneviratne et al., 2010). Therefore, integrated observations of soil water content and the exchange of water and heat between the soil, vegetation, and atmosphere are critical to improve our understanding of the terrestrial system response to changes in climatic conditions and land management (Dirnbock et al., 2003; Foley et al., 1998; Hinzman et al., 2005; Refsgaard, 1997; Seneviratne et al., 2010).

To this end, a network of integrated observation platforms have been established in the framework of the Terrestrial Environmental Observatories (TERENO) initiative to investigate the consequences of global change on terrestrial ecosystems (Bogena et al., 2012; Zacharias et al., 2011). TERENO aims to collect long-term data series of system states and fluxes using state-of-the-art monitoring technologies. In previous work, the comprehensive catchment monitoring within TERENO has enabled to close the local water balance (Graf et al., 2014) and to investigate of the effects of deforestation on water, energy, and matter fluxes in an integrative manner (Bogena et al., 2015). One of the highly instrumented sites within TERENO is the

Earth Syst. Sci. Data Discuss., doi:10.5194/essd-2016-14, 2016
Manuscript under review for journal Earth Syst. Sci. Data
Published: 6 June 2016

Rollesbroich headwater catchment, which is fully covered by grassland. It is located in the TERENO observatory Eifel/Lower Rhine Valley. All components of the water balance (e.g. precipitation, evapotranspiration, runoff, soil water content) are continuously monitored in the Rollesbroich catchment using state-of-the-art instrumentation, providing detailed information about the spatial and temporal variation of the local water cycle for the evaluation of hydrological models (Bloschl and Sivapalan, 1995; Thompson et al., 2011). In addition, using water balance data within the context of hydrological modelling helps to determine measurement errors, to diagnose such errors, and to avoid misattribution of water balance components (Evett et al., 2012; Kampf and Burges, 2010; Vasilenko, 2004). Finally, quantification of water balance components is helpful for understanding the availability of water resources, the potential of hydrologic extremes such as floods and droughts, and the interactions between the land surface and the atmosphere (Flerchinger and Cooley, 2000; Huntington, 2006).

Here, we present a comprehensive hydrological data set recorded in the Rollesbroich catchment from 1st May 2011 to 31st December 2013. The hydrological data set includes time series of meteorological forcing (i.e. precipitation, air temperature, air humidity, radiation components, and wind speed), actual evapotranspiration, runoff, as well as soil water content data from a wireless sensor network (SoilNet). In addition, information on soil physical properties and vegetation (i.e. Leaf Area Index, LAI) useful for the parameterization of hydrological models is presented.

Earth Syst. Sci. Data Discuss., doi:10.5194/essd-2016-14, 2016
Manuscript under review for journal Earth Syst. Sci. Data
Published: 6 June 2016

2. Catchment description

The Rollesbroich catchment (50°37'27''N, 6°18'17''E) is located in the Eifel and covers an area of about 40 ha with altitudes ranging from 474 to 518 m.a.s.l. The catchment mean annual air temperature and precipitation are 7.7 °C and 103.3 cm, respectively, for the period from 1981 to 2001. These data are recorded by a meteorological station operated by the North Rhine-Westphalian State Environment Agency with a distance of 4 km from the Rollesbroich catchment. The dominant soils are Cambisols in the southern part and Stagnosols in the northern part of the catchment. The grassland vegetation is dominated by perennial ryegrass (Lolium perenne) and smooth meadow grass (Poa pratensis). The average slope within the hydrological observatory is 1.63° (min.: 0.35°, max.: 3.12°).

3. Methods

3.1 Meteorological data

Meteorological data, i.e. precipitation, air temperature, air humidity, radiation components, and wind speed, were recorded at a micrometeorological tower located in the center of the almost flat terrain in the southern part of the Rollesbroich catchment (see Figure 1). Wind speed was obtained with a sonic anemometer at 2.6 m above surface (CSAT3, Campbell Scientific, Inc., Logan, USA). The H_2O concentration was measured using an open-path infrared gas analyzer (LI7500, LI-COR Inc., Lincoln, NE, USA) at the same height. Air temperature and humidity (HMP45C, Vaisala Inc., Helsinki, Finland) were measured at 2.6 m height above the ground surface. Incoming short- and longwave radiation were determined using a NR01 four-component net radiometer (Hukseflux Thermal Sensors, Delft, Netherlands). Data of all instruments including diagnostic data was recorded with a logger (CR3000, Campbell Scientific, Logan, UT,

Earth Syst. Sci. Data Discuss., doi:10.5194/essd-2016-14, 2016
Manuscript under review for journal Earth Syst. Sci. Data
Published: 6 June 2016

Open Access Earth System Science Data Discussions

USA) at 20 Hz. Precipitation was recorded by a heated Hellmann type tipping bucket rain gauge (eco-Tech GmbH, Bonn, Germany). In July 2013, a weight-based precipitation gauge (Pluvio^2, OTT Hydromet GmbH, Kempten, Germany) was added to the nearby backup climate station, providing more accurate measurements of all precipitation types. Both precipitation gauges were installed at a height of 1 m above ground surface as recommended by the German Weather Service for elevations larger than 500 m a.s.l. and occasional heavy snowfall. All meteorological measurements were stored at 10 min intervals.

3.2 Actual evapotranspiration

Latent heat flux was obtained by the eddy covariance (EC) technique. The EC post processing software TK3.1 (Mauder and Foken, 2011) was used to calculate latent heat flux from the vertical wind velocity obtained by the sonic anemometer (CSAT3, Campbell Scientific, Inc., Logan, USA) and water vapor density obtained by an infrared gas analyzer (LI7500, LI-COR Inc., Lincoln, NE, USA). The processing and quality assurance of the EC data followed the corresponding TERENO strategy presented in Mauder (2013). After receiving latent heat flux, actual evapotranspiration was calculated using:

$$ET_a = \frac{LH}{\rho_w * L_{water}} \qquad \text{Eq. 1}$$

$$L_{water} = 10^{-3} * (2500.8 - 2.36 * T + 0.0016 * T^2 - 0.00006 * T^3) \qquad \text{Eq. 2}$$

where ET_a is actual evapotranspiration (m s^{-1}), LH is latent heat flux (W m^{-2}), ρ_w is water density (kg m^{-3}), L_{water} is latent heat of condensation of water in the temperature range from -25 to 40 °C (J kg^{-1}), and T is air temperature (°C).

3.3 Runoff

Runoff is measured at the catchment outlet using a gauging station equipped with a combination of a V-notch weir for low flow measurements and a Parshall flume to measure normal to high flows. Runoff data of the two weir types are combined by using V-notch values for water levels below 5 cm, Parshall flume values for water levels greater than 10 cm and the weighted mean of V-notch and Parshall flume values for water levels between 5 and 10 cm, where the water levels refer to those of the V-notch weir.

3.4 Soil water content

Soil water content was at 87 SoilNet locations within the southern part of catchment (Figure 1) using SPADE soil moisture sensors (Qu et al., 2013; Hübner et al., 2009). The SPADE sensors were vertically installed at 5 cm, 20 cm and 50 cm depth. Two SPADE sensors were installed in parallel at each depth with a distance of ~10 cm to increase the sensing volume and to allow examination of inconsistencies in sensor reading. The measurement frequency was 15 min.

The SPADE sensor is a ring oscillator. The oscillator frequency is a function of the dielectric permittivity of the surrounding medium (Qu et al., 2013), which strongly depends on the water content of the soil because of the high permittivity of water ($\varepsilon_w \approx 80$) as compared to mineral soil solids ($\varepsilon_s \approx 2$~9), and air ($\varepsilon_a \approx 1$). The temperature of the soil was also determined by the SPADE sensor using a digital thermometer (DS18B20) with an accuracy of ±0.5 °C in the range from -10 to 85 °C. The two-step calibration procedure suggested by Jones et al. (2005) was used to relate sensor reading to soil moisture. In a first step, reference liquids with a known dielectric

Earth Syst. Sci. Data Discuss., doi:10.5194/essd-2016-14, 2016
Manuscript under review for journal Earth Syst. Sci. Data
Published: 6 June 2016

permittivity were used to calibrate the following empirical model (Eq. 3) that relates sensor reading to apparent dielectric permittivity:

$$K_a = \gamma + \frac{1}{\alpha + {}^{\beta}/_{v}} \qquad \text{Eq. 3}$$

where K_a is the dielectric permittivity, α, β, and γ are the fitting parameters, and v is sensor output (unit, V). Prior to installation, 60 SPADE sensors were calibrated in five reference liquids that covered a permittivity range from 2.2 to 34.8. The outputs for the 60 sensors as well as the fitted model are shown in Figure 2. The root mean square error (RMSE) between known and predicted dielectric permittivity was 0.0188, and the best fitting parameters of α, β, and γ were -0.1502, 0.3612, and -0.1599, respectively.

In a second step, a site-specific calibration between dielectric permittivity and soil water content was obtained using a complex refraction index model (CRIM, Eq. 4) as proposed by Birchak et al. (1974):

$$\theta = \frac{K_a{}^{0.5} - (1-\eta) * K_{solid}^{0.5} - \eta * K_{air}^{0.5}}{K_{water}^{0.5} - K_{air}^{0.5}} \qquad \text{Eq. 4}$$

where η is the porosity of the soil, 1-η is the solid fraction, K_a is the permittivity of soil, and K_{water}, K_{solid}, and K_{air} are the permittivity of water, solids, and air component of soil, respectively. In order to estimate the unknown value of K_{solid} and to assess the accuracy of this relationship, 15 undisturbed samples (length = 7.7 cm, diameter = 5 cm) were taken from the two main soil types in 5, 20 and 50 cm depth. These samples were first saturated with deionized water and then CS 640-L 3-rod TDR probes with a length of 7.5 cm were inserted in the middle of the sample. These probes were connected to a TDR100 system (Campbell Scientific, Inc., Logan, USA) to determine the dielectric permittivity of the soil samples using a custom-made MatLab algorithm based on the travel time analysis algorithm (Heimovaara and Bouten, 1990). Subsequently, the samples were dried and both weight and dielectric permittivity of each sample were determined in regular time intervals. After drying at room temperature, the remaining water was removed by oven-drying at 105 °C for 24 hours so that the dry bulk density, porosity, and the volumetric soil water content could be determined from the recorded weights.

The measured dielectric permittivity and soil water content and the fitted relationships are shown in Figure 3. Because of the large difference in porosity at the three depths, the mean porosity at each depth was determined from the calibration samples and used to parameterize three different relationships. After fitting the solid permittivity for each depth, the performance of these calibration relationships was judged by the RMSE (Table 1). It was found that the three relationships performed well with a RMSE ranging from 0.022 to 0.028 $cm^3\ cm^{-3}$.

As already briefly discussed in Qu et al. (2014), we found that sensor output showed pronounced diurnal variations after the deployment of the sensor network. This behavior was attributed to a charging capacitor that affected the first reading of the SPADE sensor. If multiple sensor readings were made sequentially without turning off the sensor, the stability of the measurement considerably improved and the temperature dependence of the measurements disappeared (Qu et al., 2014). To correct these temperature-dependent oscillations in sensor reading, the acquisition software of SoilNet was changed temporarily so that two measurements were saved from 5th September 2012 to 3th March 2013. After 3th March 2013, the software was updated again so that only the second more accurate measurement was saved. Figure 4 shows an example of the measured voltage for the first and second measurements and the soil temperature for a selected sensor (location 053, 5 cm depth). It can be seen that the difference between the two measurements (Δv) is strongly correlated with soil temperature and could be fitted with a second order empirical polynomial with a RMSE of 5.18 mV (Figure 5). Such second-order polynomial functions were obtained for all sensors individually and subsequently used to correct measurements made between April 2011 and September 2012. After the correction, measurements from the closely-spaced sensors at a single measurement location agreed well with each other with a RMSE that varied from 0.010 to 0.035 $cm^3\ cm^{-3}$. The uncorrected and corrected voltage as well as the associated soil water content for the selected sensor is plotted in Figure 6. It is clear that the corrected measurements before September 2012 better match the expected soil water content after September 2012. On average, the corrected soil water content was 0.07 $cm^3\ cm^{-3}$ lower than the uncorrected values. The plausibility of the corrected soil water content values is further supported by the fact that the unexpected increase in soil water content in the winter of 2012 disappeared after the temperature correction. The corrected soil water content is now relatively constant in winter and the maximum of the soil water content corresponds well with the porosity determined from the soil samples (both 0.59 $cm^3\ cm^{-3}$).

3.5 Soil physical properties

Soil cores were taken at all locations where soil water content sensors were installed (length: 100 cm, diameter 8 cm; Carl Hamm GmbH, Essen, Germany). Then, soil samples were taken from three pedological horizons (0-10, 10-20, and 20-40 cm) within the soil cores (see Figure 1), which resulted in a total of 282 soil samples. Sand, silt, and clay fractions were determined using a combination of wet sieving (sand fractions) and sedimentation (silt and clay fraction) following

Earth Syst. Sci. Data Discuss., doi:10.5194/essd-2016-14, 2016
Manuscript under review for journal Earth Syst. Sci. Data
Published: 6 June 2016

ISO-11277 (2009). Total carbon content (C) and nitrogen content (N) were analyzed on sieved (<2 mm) and grounded samples by elemental analysis, and complemented with mid-infrared spectroscopy (ISO-10694, 1995). More details of the soil laboratory analyses can be found at Schiedung et al. (2015).

3.6 Leaf area index

The agricultural management of the different fields in the Rollesbroich catchment is very similar. Heterogeneity of the grass cover is mainly caused by different mowing times, which typically vary only by a few days. Therefore, we assume that the grass cover is homogeneous on the long-term in the Rollesbroich catchment. The effective leaf area index (LAI_{eff}) that contributes to actual evapotranspiration was computed from grass height, h, using the following equations (Allen et al., 2006; Rochette et al., 1991):

$$LAI = 24 * h \qquad \text{Eq. 5}$$

$$LAI_{eff} = \frac{LAI}{0.3 * LAI + 1.2} \qquad \text{Eq. 6}$$

Average grass height in the Rollesbroich catchment was determined weekly by measuring grass height at five representative locations in the catchment.

Time series of LAI were also derived from RapidEye images using the normalized difference vegetation index (NDVI) approach (Myneni et al., 1997). The NDVI is calculated from infra-red (NIR) and red-edge spectral bands. The NDVI of a plant with high LAI has a high ratio between NIR and red reflectance that can be detected by RapidEye. The LAI was computed from the

Earth Syst. Sci. Data Discuss., doi:10.5194/essd-2016-14, 2016
Manuscript under review for journal Earth Syst. Sci. Data
Published: 6 June 2016

NDVI values using a radiative transfer model (Myneni et al., 1997). Detailed information about the procedure can be found in Ali et al (2013).

4. Data management and quality control

The distributed spatial data infrastructure TEODOOR (http://www.tereno.net) was developed to handle, describe, exchange, and publish all monitored environmental data of the TERENO project (Kunkel et al., 2013). Each institution hosting an individual observatory maintains its local data infrastructure. The observatories are connected via OGC-compliant web-services, while the TERENO Data Discovery Portal (DDP) as a central application enables data searching, visualization and download. According to the TERENO Policy it is obligated, that each dataset is described by standardized metadata elements, like ISO19115, OGC SensorML or NetCDF's CF-Conventions.

The observation datasets are processed and assessed within TEODOOR three different ways (for details see Devaraju et al., 2015). In first the data processing type, the imported data undergoes automated quality checks (e.g., minimum/maximum thresholds) and subsequently are published after visual inspection by experts. For example data from weather stations and river gauges are processed in this way. Secondly, more complex data can be externally processed and assessed by the principal investigators and subsequently imported into TEODOOR, e.g., eddy flux data. The third data processing type involves also automatic data import, but in this case the data quality assessment is executed using an external evaluation method developed by the responsible scientist, e.g. wireless sensor network data. Subsequently, the flagging information is updated by TEODOOR after the quality assessment has been completed.

Characterization of data quality is done by three descriptors, which are stored together with each observation: data uncertainty, data processing levels and data quality flags. The observed data values remain unchanged in any case. Data uncertainty arises from the observation process itself and is mainly determined by the accuracy of the sensors used. Data processing levels indicate the status of data handling. For instance, (unpublished) raw data is termed 'level 1', 'level 2' refers to data subjected to quality control, whereas the higher levels refer to derived data products. The flagging scheme consists of two tiers: the first tier includes generic flags, e.g., 'good', 'unevaluated', 'suspicious' or 'bad'. The second tier is use-case-specific and indicates either the result of individual quality tests, e.g., failed gradient checks, or background events affecting data values, e.g., icing events.

In the following, we present in more detail how data was checked for plausibility to derive the data sets used in this study.

4.1 Meteorological data and latent heat flux

Meteorological data was checked for quality by a multi step quality control including the use of diagnostic information provided by the instruments, the application of site specific plausibility limits, visual inspections of the data series and cross checks with data from the nearby backup weather station. The quality control of the latent heat flux was in accordance with the standardized method for the processing and quality assessment of eddy covariance data as suggested by Mauder et al. (2013). This scheme includes site-specific plausibility limits and the application of a spike removal algorithm based on median absolute deviation of raw measurements. Processed half-hourly fluxes and statistics were checked using three different flags (high, moderate, and low) based on tests of integral turbulence and stationarity (Foken and

Wichura, 1996). In this study, only data of high and moderate quality were used. A more detailed description of the treatment of eddy covariance data can be found elsewhere (Gebler et al., 2015; Post et al., 2015).

4.2 Runoff

The gauging stations consist of a V-notch weir and a Parshall flume. As a first quality check, time series of both gauge types were compared for consistency. In addition, both runoff time series were visually inspected for inexplicable outliers (e.g. runoff peak without preceding rainfall event) and sensor failures. As outlined above, unreliable data were identified and appropriate flags were set.

4.3 Soil water content

Measurements of soil moisture outside the physical plausibility range (0.05 to 0.85 cm^3cm^{-3}) were identified and flagged. Subsequently, unreliable measurements were identified by analyzing the first derivative of the soil water content time series. In case an increase larger than two times the standard deviations of the preceding 24 hours was observed, this measurement was flagged as an unreliable measurement. In addition, the whole data set was visually inspected to verify the results of the automatic flagging procedures.

5. Data sets

5.1 Hydrometeorological data

Temporal dynamics of the most important meteorological data (i.e. air temperature, air humidity, radiation components, wind speed, precipitation, actual evapotranspiration, and runoff) and water balance components (i.e. precipitation, actual evapotranspiration, runoff, and soil water content) from 1st May 2011 to 31st December 2013 are plotted in Figure 7 and Figure 8. The air temperature, relative humidity, short wave radiation, and evapotranspiration showed a clear annual pattern. The highest runoff amounts occurred during the winter seasons due to high precipitation amounts and low evapotranspiration rates, as well as overland flow due to saturation excess (Figure 8). Generally, soil water content showed a strong dependence on precipitation events especially at 5 and 20 cm depth. Quick increases in soil water content can be observed after rainfall events, which were followed by a slow recession during periods without precipitation.

5. 2 Water balance closure

The water balance can be written as:

$$P = R + ET_a + \Delta S \qquad \text{Eq. 7}$$

where P is precipitation, R is runoff, ET_a is actual evapotranspiration, and ΔS is the storage term. Because of the relatively low hydraulic conductivity (10^{-9} to 10^{-7} ms^{-1}) of the aquifer bedrock (HK100, 2009), we neglected deep percolation. Mean average annual precipitation was partitioned into about 57% evapotranspiration and 50% runoff. The residual of the balance was within 7% of precipitation for the whole time period as shown in Figure 8. This residual is related to measurement uncertainty and soil water storage depletion. As presented by Graf et al. (2014), soil water storage can be derived from the measured soil water content, θ, as follows:

$$S(t) = \int \theta(x, y, z, t)dxdydzdt \approx \sum_{i=1}^{N} c_i \theta(i, t) + \varepsilon \qquad \text{Eq. 8}$$

where t is time, z is depth, the integral refers to the 3D domain as defined by the catchment boundary. The discrete version of storage is expressed by the right-hand side of the equation, where i is the number of sensors, and c_i is the empirical coefficient representing the 3D domain which is well represented by the sensor. The residual of ε is the storage affected by vegetation or groundwater and not represented well by the sensor. The changes in ΔS are expected to correspond well with the residual of the major water budget component, P-ET_a-R (Eq. 7). Thus, the time derivative of soil water storage should be linearly related to this residual, although measurement errors within the other water balance components and the unaccounted storage terms (e.g. vegetation storage) will deteriorate this relation. Our results show that there is a linear relationship between the derivative of soil water content and the water balance residual (Figure 9). The R^2 is 0.60, which means that 60% of the residual of the water balance is explained by soil water storage changes in the catchment.

5.3 Soil physical properties

The mean and standard deviation of %sand, %silt, % clay, organic carbon content, and bulk density are shown in Table 2. The bulk density ranged from 0.94 g cm^{-3} to 1.52 g cm^{-3} and generally increased with depth. Porosity ranged from 0.43 cm^3 cm^{-3} to 0.65 cm^3 cm^{-3} and decreased with depth. The higher spatial variability of porosity of the subsoil is caused by the higher and more variable stone content at this depth. In addition, former agriculture land

Earth Syst. Sci. Data Discuss., doi:10.5194/essd-2016-14, 2016
Manuscript under review for journal Earth Syst. Sci. Data
Published: 6 June 2016

management activities reduced the spatial variability of porosity of the top soil (plough layer, 20 to 30 cm thick). The measured soil texture fractions and soil density were used to estimate the spatial distribution of soil hydraulic properties with the pedotransfer function Rosetta (Schaap et al., 2001). Figure 10 shows the spatial distribution of Mualem-van Genuchten soil hydraulic parameters (van Genuchten, 1980) derived with Rosetta at 5 cm depth. Some soil hydraulic parameter show a distinct pattern. For instance, the VGM parameter α is generally larger in the northern part than in the southern part of the catchment. Such information is important for the investigation of controlling factors of spatial patterns of soil water content.

5.4 Leaf area index

The LAI derived from measured grass height agrees well with the LAI obtained from RapidEye images (Figure 11). Both LAI time series showed a distinct annual pattern with the highest values during the summer time. We averaged the monthly LAI derived from measured grass height and an ANOVA was conducted to test whether there was a significant difference between the LAI obtained from grass height and RapidEye in the time period of May to December in 2011. The results of this ANOVA (Table 3) confirmed that there is no significant difference between the two methods to determine LAI.

6 Conclusions and data access

We presented data from the intensively instrumented hydrological observatory Rollesbroich providing long-term hydrometeorological data with high spatial and temporal resolution. Our results showed that the catchment water balance is reasonably closed by the provided measurements, and that 60% of the water balance residual could be related to soil water storage changes within the Rollesbroich catchment. In addition, important soil physical and chemical properties (e.g. hydraulic properties) have been reported in addition to catchment-scale information on vegetation. This comprehensive hydrological data set can be used for the calibration, validation and improvement of hydrological models, e.g. in hydrological model intercomparison projects (Breuer et al., 2009; Maxwell et al., 2014; Refsgaard, 1997; Smith et al., 2004) and for the calibration and validation of remote sensing data products (Bastiaanssen et al., 1998; Jackson et al., 2010; Le Hegarat-Mascle et al., 2002; Njoku et al., 2003). All the data are freely available from the TERENO data portal (http://www.tereno.net). In addition, three persistent identifiers are associated with the data set described here:

- Climate/Runoff/Water Quality station: http://doi.org/10.5880/TERENO.2016.001
- EC/Climate station Rollesbroich 3: http://doi.org/10.5880/TERENO.2016.002
- SoilNet Rollesbroich: http://doi.org/10.5880/TERENO.2016.003

Acknowledgments

We gratefully acknowledge the support of the SFB-TR32 "Pattern in Soil–Vegetation–Atmosphere Systems: Monitoring, Modeling and Data Assimilation" funded by the Deutsche Forschungsgemeinschaft (DFG), and TERENO funded by the Helmholtz-Gemeinschaft. Martina Kettler and Daniel Dolfus are thanked for supporting the acquisition of vegetation information. Henning Schiedung from Bonn University is thanked for analyzing and providing the soil texture information.

Earth Syst. Sci. Data Discuss., doi:10.5194/essd-2016-14, 2016
Manuscript under review for journal Earth Syst. Sci. Data
Published: 6 June 2016

References

Ali, M., Montzka, C., Stadler, A., Menz, G., Vereecken, H., 2013. Estimation and validation of leaf area index time series for crops on 5m scale from space. International Geosciences and Remote Sensing Symposium (IGARSS), Melbourne, Australia, 21-26 July 2013.

Albertson, J. D., and Kiely, G., 2001, On the structure of soil moisture time series in the context of land surface models: Journal of Hydrology, v. 243, no. 1-2, p. 101-119.

Allen, R. G., Pruitt, W. O., Wright, J. L., Howell, T. A., Ventura, F., Snyder, R., Itenfisu, D., Steduto, P., Berengena, J., Yrisarry, J. B., Smith, M., Pereira, L. S., Raes, D., Perrier, A., Alves, I., Walter, I., and Elliott, R., 2006, A recommendation on standardized surface resistance for hourly calculation of reference eto by the fao56 penman-monteith method: Agricultural Water Management, v. 81, no. 1-2, p. 1-22.

Bastiaanssen, W. G. M., Pelgrum, H., Wang, J., Ma, Y., Moreno, J. F., Roerink, G. J., and van der Wal, T., 1998, A remote sensing surface energy balance algorithm for land (sebal) - 2. Validation: Journal of Hydrology, v. 212, no. 1-4, p. 213-229.

Betts, A. K., Ball, J. H., Beljaars, A. C. M., Miller, M. J., and Viterbo, P. A., 1996, The land surface-atmosphere interaction: A review based on observational and global modeling perspectives: Journal of Geophysical Research-Atmospheres, v. 101, no. D3, p. 7209-7225.

Birchak, J. R., Gardner, C. G., Hipp, J. E., and Victor, J. M., 1974, High dielectric constant microwave probes for sensing soil moisture: Proceedings of the Ieee, v. 62, no. 1, p. 93-98.

Bloschl, G., and Sivapalan, M., 1995, Scale issues in hydrological modeling - a review: Hydrological Processes, v. 9, no. 3-4, p. 251-290.

Bogena, H., Kunkel, R., Pütz, T., Vereecken, H., Krüger, E., Zacharias, S., Dietrich, P., Wollschläger, U., Kunstmann, H., Papen, H., Schmid, H. P., and Munch, J. C., 2012, Tereno – long-term monitoring network for terrestrial research: Hydrologie und Wasserbewirtschaftung, v. 56, no. 3, p. 138-143.

Bogena, H. R., Bol, R., Borchard, N., Brueggemann, N., Diekkrueger, B., Druee, C., Groh, J., Gottselig, N., Huisman, J. A., Luecke, A., Missong, A., Neuwirth, B., Puetz, T., Schmidt, M., Stockinger, M., Tappe, W., Weihermueller, L., Wiekenkamp, I., and Vereecken, H., 2015, A terrestrial observatory approach to the integrated investigation of the effects of deforestation on water, energy, and matter fluxes: Science China-Earth Sciences, v. 58, no. 1, p. 61-75.

Breuer, L., Huisman, J. A., Willems, P., Bormann, H., Bronstert, A., Croke, B. F. W., Frede, H. G., Graeff, T., Hubrechts, L., Jakeman, A. J., Kite, G., Lanini, J., Leavesley, G., Lettenmaier, D. P., Lindstroem, G., Seibert, J., Sivapalan, M., and Viney, N. R., 2009, Assessing the impact of land use change on hydrology by ensemble modeling (luchem). I: Model intercomparison with current land use: Advances in Water Resources, v. 32, no. 2, p. 129-146.

Crow, W. T., Ryu, D., and Famiglietti, J. S., 2005, Upscaling of field-scale soil moisture measurements using distributed land surface modeling: Advances in Water Resources, v. 28, no. 1, p. 1-14.

Devaraju, A, Jirka, S., Kunkel, R. Sorg, J., 2015, Q-SOS - A Sensor Observation Service for Accessing Quality Descriptions of Environmental Data, SPRS Int. J. Geo-Inf. 2015, 4(3), 1346-1365; doi:10.3390/ijgi4031346.

Dirnbock, T., Dullinger, S., and Grabherr, G., 2003, A regional impact assessment of climate and land-use change on alpine vegetation: Journal of Biogeography, v. 30, no. 3, p. 401-417.
Evett, S. R., Schwartz, R. C., Casanova, J. J., and Heng, L. K., 2012, Soil water sensing for water balance, et and wue: Agricultural Water Management, v. 104, p. 1-9.
Flerchinger, G. N., and Cooley, K. R., 2000, A ten-year water balance of a mountainous semi-arid watershed: Journal of Hydrology, v. 237, no. 1-2, p. 86-99.
Foken, T., and Wichura, B., 1996, Tools for quality assessment of surface-based flux measurements: Agricultural and Forest Meteorology, v. 78, no. 1-2, p. 83-105.
Foley, J. A., Levis, S., Prentice, I. C., Pollard, D., and Thompson, S. L., 1998, Coupling dynamic models of climate and vegetation: Global Change Biology, v. 4, no. 5, p. 561-579.
Fratini, G., and Mauder, M., 2014, Towards a consistent eddy-covariance processing: An intercomparison of eddypro and tk3: Atmospheric Measurement Techniques, v. 7, no. 7, p. 2273-2281.
Gebler, S., Hendricks Franssen, H. J., Pütz, T., Post, H., Schmidt, M., and Vereecken, H., 2015, Actual evapotranspiration and precipitation measured by lysimeters: A comparison with eddy covariance and tipping bucket: Hydrology and Earth System Sciences, v. 19, p. 2145-2161.
Graf, A., Bogena, H. R., Druee, C., Hardelauf, H., Puetz, T., Heinemann, G., and Vereecken, H., 2014, Spatiotemporal relations between water budget components and soil water content in a forested tributary catchment: Water Resources Research, v. 50, no. 6, p. 4837-4857.
Heimovaara, T. J., and Bouten, W., 1990, A computer-controlled 36-channel time domain reflectometry system for monitoring soil-water contents: Water Resources Research, v. 26, no. 10, p. 2311-2316.
Hinzman, L. D., Bettez, N. D., Bolton, W. R., Chapin, F. S., Dyurgerov, M. B., Fastie, C. L., Griffith, B., Hollister, R. D., Hope, A., Huntington, H. P., Jensen, A. M., Jia, G. J., Jorgenson, T., Kane, D. L., Klein, D. R., Kofinas, G., Lynch, A. H., Lloyd, A. H., McGuire, A. D., Nelson, F. E., Oechel, W. C., Osterkamp, T. E., Racine, C. H., Romanovsky, V. E., Stone, R. S., Stow, D. A., Sturm, M., Tweedie, C. E., Vourlitis, G. L., Walker, M. D., Walker, D. A., Webber, P. J., Welker, J. M., Winker, K., and Yoshikawa, K., 2005, Evidence and implications of recent climate change in northern alaska and other arctic regions: Climatic Change, v. 72, no. 3, p. 251-298.
HK100, 2009, Hydrogeological map of north rehine-westphalia (1:100 000): Geological Survey, North Rehine-Westphalia, Krefeld, Germany.
Hübner, C., Cardell-Oliver, R., Becker, R., Spohrer, K., Jotter, K., and Wagenknecht, T., 2009, Wireless soil moisture sensor networks for environmental monitoring and vineyard irrigation: Helsinki University of Technology, no. 1, p. 408-415.
Huntington, T. G., 2006, Evidence for intensification of the global water cycle: Review and synthesis: Journal of Hydrology, v. 319, no. 1-4, p. 83-95.
ISO-10694, 1995, Soil quality – determination of organic and total carbon after dry combustion 606 (elemental analysis). Beuth, berlin.
ISO-11277, 2009, Soil quality – determination of particle size distribution in mineral soil material – 608 method by sieving and sedimentation. Beuth, berlin.
Jackson, T. J., Cosh, M. H., Bindlish, R., Starks, P. J., Bosch, D. D., Seyfried, M., Goodrich, D. C., Moran, M. S., and Du, J., 2010, Validation of advanced microwave scanning radiometer soil moisture products: Ieee Transactions on Geoscience and Remote Sensing, v. 48, no. 12, p. 4256-4272.

Earth Syst. Sci. Data Discuss., doi:10.5194/essd-2016-14, 2016
Manuscript under review for journal Earth Syst. Sci. Data
Published: 6 June 2016

Jaeger, E. B., and Seneviratne, S. I., 2011, Impact of soil moisture-atmosphere coupling on european climate extremes and trends in a regional climate model: Climate Dynamics, v. 36, no. 9-10, p. 1919-1939.

Jones, S. B., Blonquist, J. M., Robinson, D. A., Rasmussen, V. P., and Or, D., 2005, Standardizing characterization of electromagnetic water content sensors: Part 1. Methodology: Vadose Zone Journal, v. 4, no. 4, p. 1048-1058.

Kampf, S. K., and Burges, S. J., 2010, Quantifying the water balance in a planar hillslope plot: Effects of measurement errors on flow prediction: Journal of Hydrology, v. 380, no. 1-2, p. 191-202.

Kunkel, R., Sorg, J., Eckardt, R., Kolditz, O., Rink, K., and Vereecken, H., 2013, Teodoor: A distributed geodata infrastructure for terrestrial observation data: Environmental Earth Sciences, v. 69, no. 2, p. 507-521.

Le Hegarat-Mascle, S., Zribi, M., Alem, F., Weisse, A., and Loumagne, C., 2002, Soil moisture estimation from ers/sar data: Toward an operational methodology: Ieee Transactions on Geoscience and Remote Sensing, v. 40, no. 12, p. 2647-2658.

Mauder, M., Cuntz, M., Druee, C., Graf, A., Rebmann, C., Schmid, H. P., Schmidt, M., and Steinbrecher, R., 2013, A strategy for quality and uncertainty assessment of long-term eddy-covariance measurements: Agricultural and Forest Meteorology, v. 169, p. 122-135.

Maxwell, R. M., Putti, M., Meyerhoff, S., Delfs, J.-O., Ferguson, I. M., Ivanov, V., Kim, J., Kolditz, O., Kollet, S. J., Kumar, M., Lopez, S., Niu, J., Paniconi, C., Park, Y.-J., Phanikumar, M. S., Shen, C., Sudicky, E. A., and Sulis, M., 2014, Surface-subsurface model intercomparison: A first set of benchmark results to diagnose integrated hydrology and feedbacks: Water Resources Research, v. 50, no. 2, p. 1531-1549.

Moncrieff, J. B., Massheder, J. M., deBruin, H., Elbers, J., Friborg, T., Heusinkveld, B., Kabat, P., Scott, S., Soegaard, H., and Verhoef, A., 1997, A system to measure surface fluxes of momentum, sensible heat, water vapour and carbon dioxide: Journal of Hydrology, v. 189, no. 1-4, p. 589-611.

Myneni, R. B., Nemani, R. R., and Running, S. W., 1997, Estimation of global leaf area index and absorbed par using radiative transfer models: Ieee Transactions on Geoscience and Remote Sensing, v. 35, no. 6, p. 1380-1393.

Njoku, E. G., Jackson, T. J., Lakshmi, V., Chan, T. K., and Nghiem, S. V., 2003, Soil moisture retrieval from amsr-e: Ieee Transactions on Geoscience and Remote Sensing, v. 41, no. 2, p. 215-229.

Post, H., Hendricks Franssen, H. J., Graf, A., Schmidt, M., and Vereecken, H., 2015, Uncertainty analysis of eddy covariance co2 flux measurements for different ec tower distances using an extended two-tower approach: Biogeosciences, v. 12, p. 1205 - 1221.

Qu, W., Bogena, H. R., Huisman, J. A., Martinez, G., Pachepsky, Y., and Vereecken, H., 2014, Effects of soil hydraulic properties on the spatial variability of soil water content: Evidence from sensor network data and inverse modeling Vadose Zone Journal, v. 13, no. 12.

Qu, W., Bogena, H. R., Huisman, J. A., and Vereecken, H., 2013, Calibration of a novel low-cost soil water content sensor based on a ring oscillator: Vadose Zone Journal, v. 12, no. 2.

Refsgaard, J. C., 1997, Parameterisation, calibration and validation of distributed hydrological models: Journal of Hydrology, v. 198, no. 1-4, p. 69-97.

Robinson, D. A., Campbell, C. S., Hopmans, J. W., Hornbuckle, B. K., Jones, S. B., Knight, R., Ogden, F., Selker, J., and Wendroth, O., 2008, Soil moisture measurement for ecological

Earth Syst. Sci. Data Discuss., doi:10.5194/essd-2016-14, 2016
Manuscript under review for journal Earth Syst. Sci. Data
Published: 6 June 2016

Open Access Earth System Science Data Discussions

and hydrological watershed-scale observatories: A review: Vadose Zone Journal, v. 7, no. 1, p. 358-389.

Rochette, P., Pattey, E., Desjardins, R. L., Dwyer, L. M., Stewart, D. W., and Dube, P. A., 1991, Estimation of maize (zea-mays-l) canopy conductance by scaling up leaf stomatal conductance: Agricultural and Forest Meteorology, v. 54, no. 2-4, p. 241-261.

Schaap, M. G., Leij, F. J., and van Genuchten, M. T., 2001, Rosetta: A computer program for estimating soil hydraulic parameters with hierarchical pedotransfer functions: Journal of Hydrology, v. 251, no. 3-4, p. 163-176.

Schiedunga H., Bornemann L., Bauke S., Welp G., Borchard N., Bogen H., and Amelung W., 2015, Spatial controls on heterotrophic respiration in a temperate grassland, Geoderma, under review.

Seneviratne, S. I., Corti, T., Davin, E. L., Hirschi, M., Jaeger, E. B., Lehner, I., Orlowsky, B., and Teuling, A. J., 2010, Investigating soil moisture-climate interactions in a changing climate: A review: Earth-Science Reviews, v. 99, no. 3-4, p. 125-161.

Smith, M. B., Seo, D. J., Koren, V. I., Reed, S. M., Zhang, Z., Duan, Q., Moreda, F., and Cong, S., 2004, The distributed model intercomparison project (dmip): Motivation and experiment design: Journal of Hydrology, v. 298, no. 1-4, p. 4-26.

Thompson, S. E., Harman, C. J., Troch, P. A., Brooks, P. D., and Sivapalan, M., 2011, Spatial scale dependence of ecohydrologically mediated water balance partitioning: A synthesis framework for catchment ecohydrology: Water Resources Research, v. 47.

van Genuchten, M. T., 1980, A closed-form equation for predicting the hydraulic conductivity of unsaturated soils: Soil Science Society of America Journal, v. 44, no. 5, p. 892-898.

Vasilenko, N. G., 2004, Water balance of small russian catchments in the southern mountainous taiga zone: "Mogot" case study, in Kane, D. L., and Yang, D., eds., Northern research basins water balance, Volume 290: Wallingford, Int Assoc Hydrological Sciences, p. 65-77.

Vereecken, H., Huisman, J. A., Bogena, H., Vanderborght, J., Vrugt, J. A., and Hopmans, J. W., 2008, On the value of soil moisture measurements in vadose zone hydrology: A review: Water Resources Research, v. 44.

Western, A. W., Grayson, R. B., and Bloschl, G., 2002, Scaling of soil moisture: A hydrologic perspective: Annual Review of Earth and Planetary Sciences, v. 30, p. 149-180.

Zacharias, S., Bogena, H., Samaniego, L., Mauder, M., Fuss, R., Puetz, T., Frenzel, M., Schwank, M., Baessler, C., Butterbach-Bahl, K., Bens, O., Borg, E., Brauer, A., Dietrich, P., Hajnsek, I., Helle, G., Kiese, R., Kunstmann, H., Klotz, S., Munch, J. C., Papen, H., Priesack, E., Schmid, H. P., Steinbrecher, R., Rosenbaum, U., Teutsch, G., and Vereecken, H., 2011, A network of terrestrial environmental observatories in germany: Vadose Zone Journal, v. 10, no. 3, p. 955-973.

Earth Syst. Sci. Data Discuss., doi:10.5194/essd-2016-14, 2016
Manuscript under review for journal Earth Syst. Sci. Data
Published: 6 June 2016

Open Access Earth System Science Data Discussions

List of Tables

Table 1. Parameters and the RMSE of the CRIM model for 5 cm, 20 cm, and 50 cm depth.

	5cm	20cm	50cm
K_{water}	78.54	78.54	78.54
K_{solid}	2.08	3.78	4.40
K_{air}	1.00	1.00	1.00
η	0.59	0.49	0.41
RMSE	0.028	0.025	0.022

Table 2. Descriptive statistics of soil properties determined from 273 soil samples taken in the Rollesbroich catchment.

		Clay %	Sand %	Silt %	Bulk density (gcm^{-3})	Carbon content (gkg^{-1})	Porosity (cm^3cm^{-3})
5 cm	mean	18.99	19.90	61.10	0.94	54.47	0.65
	std	2.00	3.82	3.79	0.12	15.82	0.05
20 cm	mean	18.03	20.76	61.20	1.28	34.08	0.52
	std	1.99	4.03	3.46	0.15	16.84	0.05
50 cm	mean	16.50	22.00	61.50	1.52	11.22	0.43
	std	2.40	5.68	4.53	0.16	6.01	0.06

Table 3. ANOVA results of LAI determination with grass height and RapidEye from May to December 2011.

Source of Variation	SS	df	MS	F	P-value	*F critical*
Variability between group	0.311	1	0.311	0.717	0.411	2.145
Variability within group	6.074	14	0.434			
Total	6.385	15				

Earth Syst. Sci. Data Discuss., doi:10.5194/essd-2016-14, 2016
Manuscript under review for journal Earth Syst. Sci. Data
Published: 6 June 2016

Open Access Earth System Science Data Discussions

List of Figures

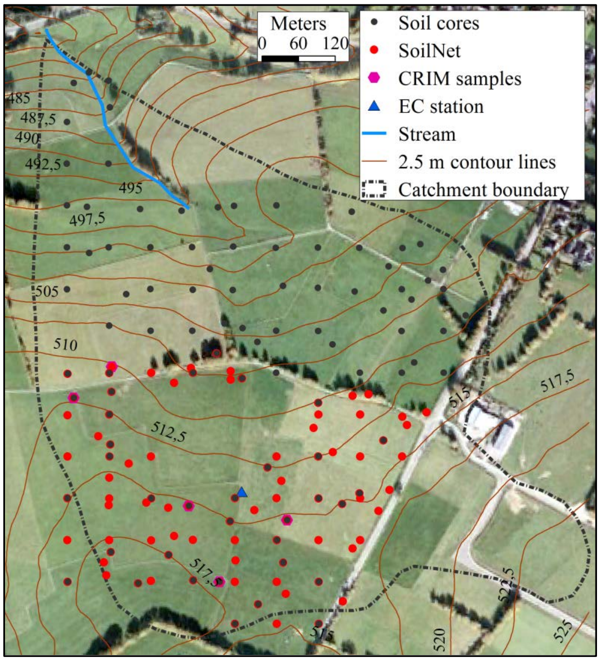

Figure 1. Map of the Rollesbroich catchment showing locations of the SoilNet sensor network, locations of the soil samples to determine soil physical and chemical properties, locations of the soil samples for site-specific calibration of the CRIM model, the location of the eddy covariance (EC) station, 2.5 m contour lines, and catchment boundary.

Earth Syst. Sci. Data Discuss., doi:10.5194/essd-2016-14, 2016
Manuscript under review for journal Earth Syst. Sci. Data
Published: 6 June 2016

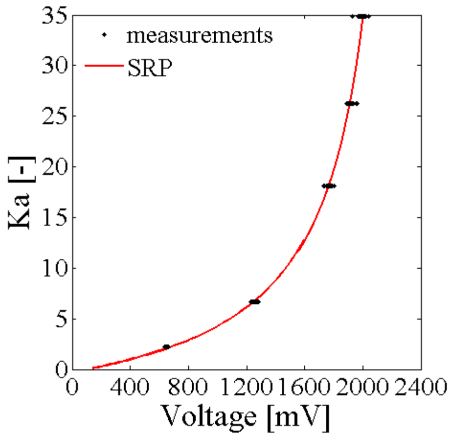

Figure 2. Sensor output of 60 SPADE sensors in five reference liquids. The fitted 'universal' calibration relationship (Eq. 3) is also presented.

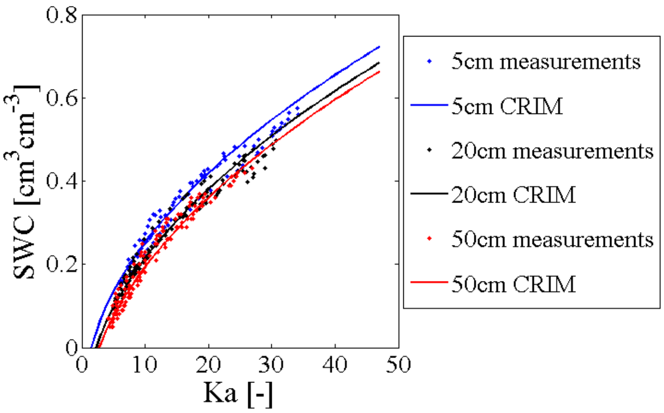

Figure 3. Relationship between dielectric permittivity and soil water content for the Rollesbroich test site and the derived K_a-θ models (CRIM).

Earth Syst. Sci. Data Discuss., doi:10.5194/essd-2016-14, 2016
Manuscript under review for journal Earth Syst. Sci. Data
Published: 6 June 2016

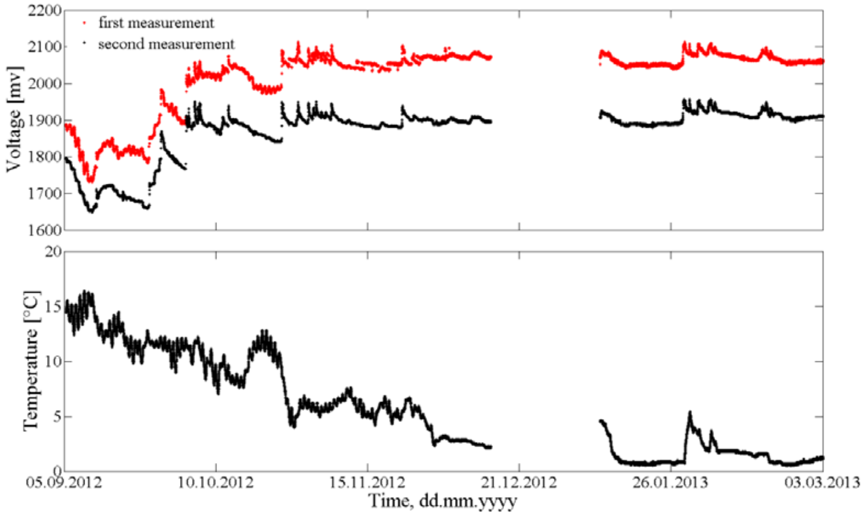

Figure 4. Time series of the first and second voltage measured after software update and the associated temperature.

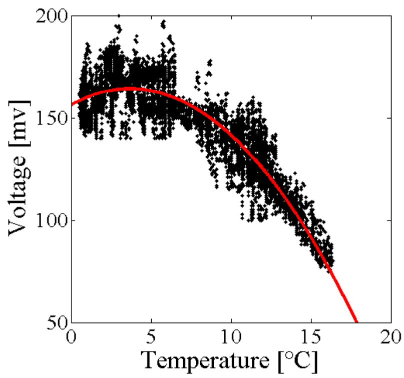

Figure 5. Second-order polynomial function fitted to the relationship between soil temperature and the difference between the first and second voltage measurements.

Earth Syst. Sci. Data Discuss., doi:10.5194/essd-2016-14, 2016
Manuscript under review for journal Earth Syst. Sci. Data
Published: 6 June 2016

Open Access Earth System Science Data Discussions

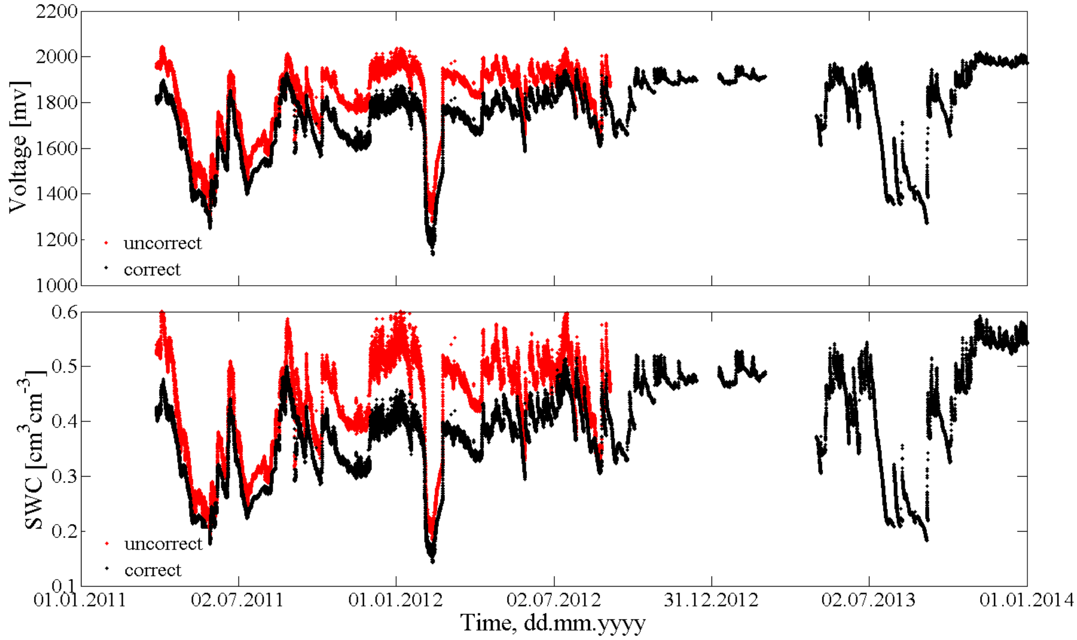

Figure 6. Uncorrected (red) and corrected (black) voltage and soil water content (SWC) measurements.

Earth Syst. Sci. Data Discuss., doi:10.5194/essd-2016-14, 2016
Manuscript under review for journal Earth Syst. Sci. Data
Published: 6 June 2016

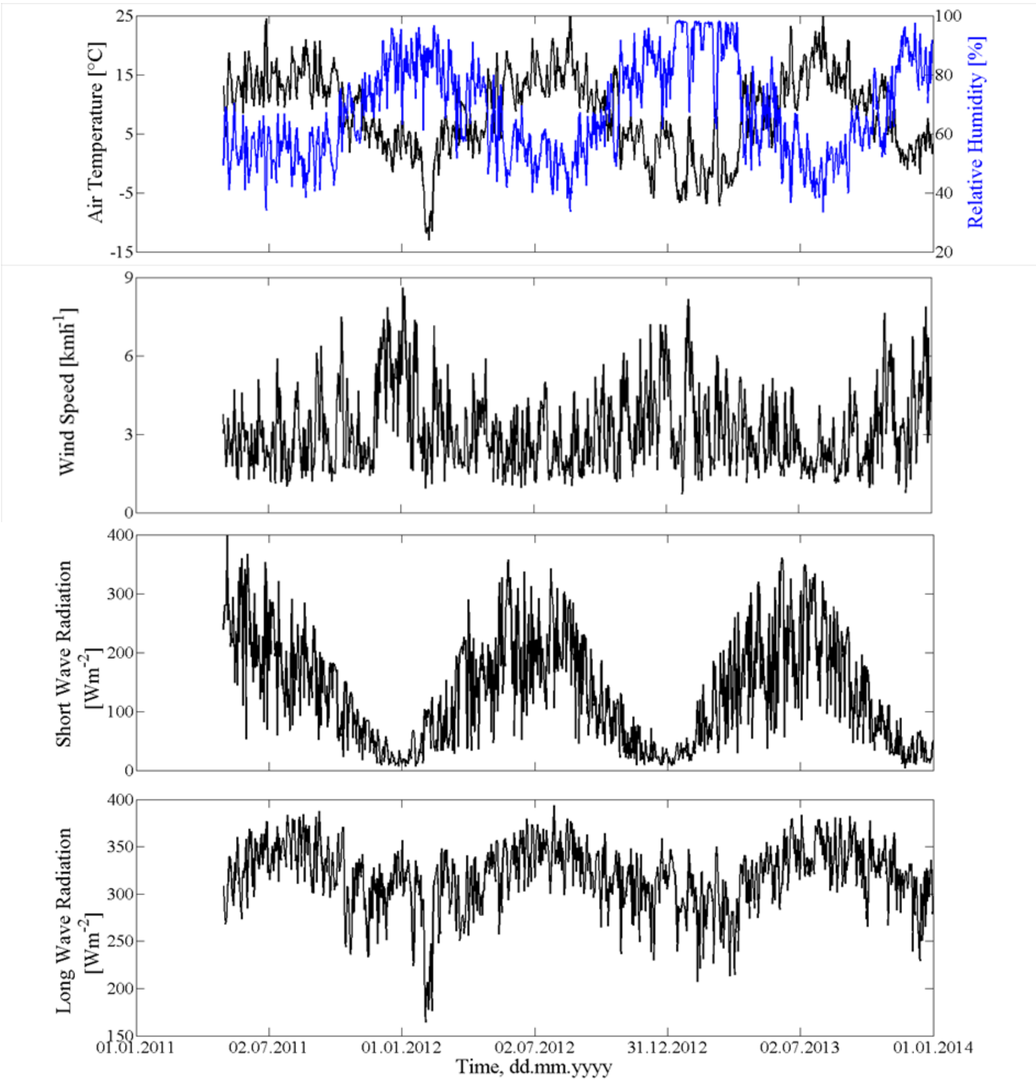

Figure 7. Daily averages of air temperature, relative humidity, wind speed, incoming short and long wave radiation measured at the eddy covariance station from 1st May 2011 to 31st December 2013.

Earth Syst. Sci. Data Discuss., doi:10.5194/essd-2016-14, 2016
Manuscript under review for journal Earth Syst. Sci. Data
Published: 6 June 2016

Open Access Earth System Science Data Discussions

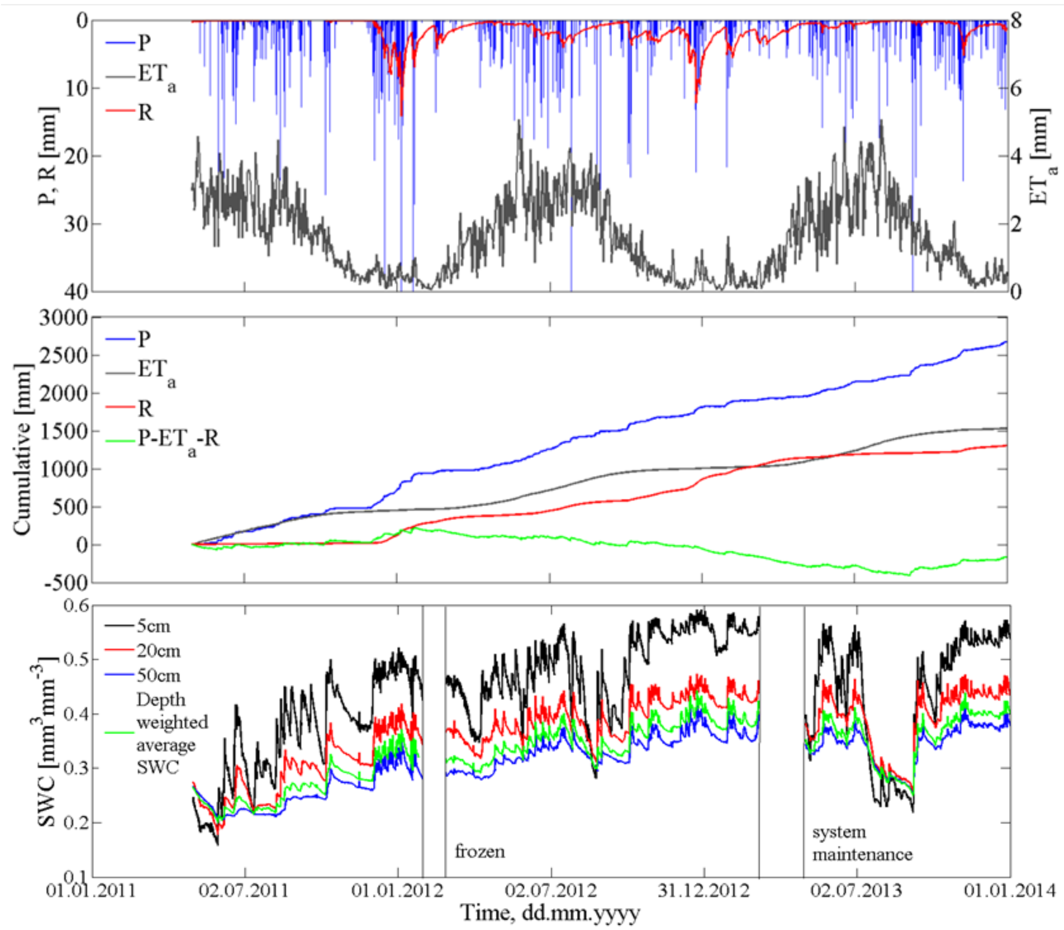

Figure 8. Daily and cumulative time series (1st May 2011 to 31st December 2013) of precipitation (P), runoff (R), actual evapotranspiration (ET_a), and spatial mean soil water content (SWC) at three depths. The SWC data contains two major gaps due to frozen soil conditions and maintenance of the SoilNet system.

Earth Syst. Sci. Data Discuss., doi:10.5194/essd-2016-14, 2016
Manuscript under review for journal Earth Syst. Sci. Data
Published: 6 June 2016

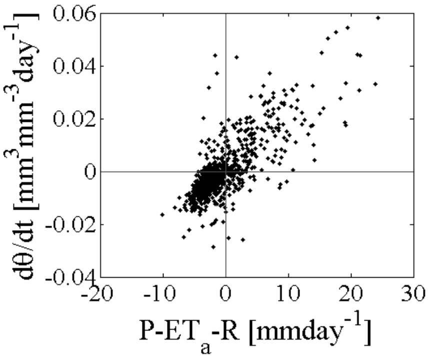

Figure 9. Time derivative of volumetric soil water content (average of all depth) versus the water balance residual.

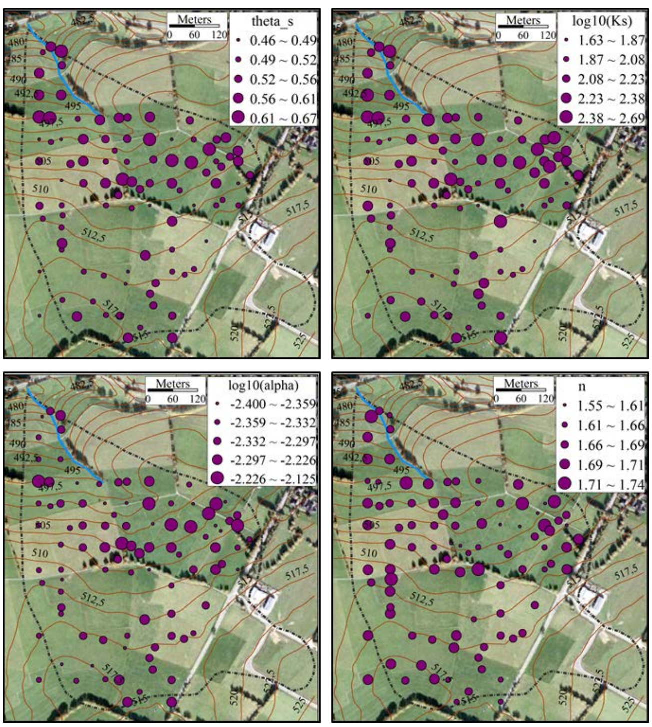

Figure 10. Spatial distribution of soil hydraulic properties (θ_s, $\log_{10}(K_s)$, $\log_{10}(\alpha)$, and n) at 5cm depth derived from soil information obtained from the soil cores taken in the Rollesbroich catchment.

Earth Syst. Sci. Data Discuss., doi:10.5194/essd-2016-14, 2016
Manuscript under review for journal Earth Syst. Sci. Data
Published: 6 June 2016

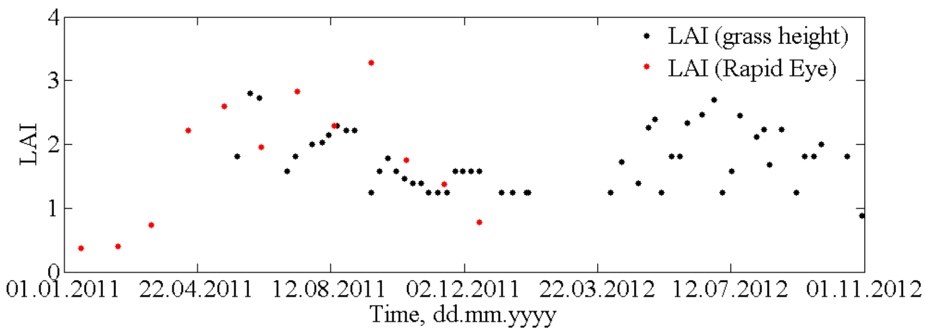

Figure 11. Time series of leaf area index (LAI) computed from measured grass height and extracted from the RapidEye images of the Rollesbroich catchment.